

High Altitude Wind Energy Generation Using Controlled Power Kites

Massimo Canale, *Member, IEEE*, Lorenzo Fagiano, *Member, IEEE*, and Mario Milanese, *Senior Member, IEEE*

Abstract—This paper presents simulation and experimental results regarding a new class of wind energy generators, denoted as **KiteGen**, which employ power kites to capture high altitude wind power. A realistic kite model, which includes the kite aerodynamic characteristics and the effects of line weight and drag forces, is used to describe the system dynamics. Nonlinear model predictive control techniques, together with an efficient implementation based on set membership function approximation theory, are employed to maximize the energy obtained by KiteGen, while satisfying input and state constraints. Two different kinds of KiteGen are investigated through numerical simulations, the *yo-yo configuration* and the *carousel configuration*, respectively. For each configuration, a generator with the same kite and nominal wind characteristics is considered. A novel control strategy for the carousel configuration, with respect to previous works, is also introduced. The simulation results show that the power generation potentials of the yo-yo and carousel configurations are very similar. Thus, the choice between these two configurations for further development of a medium-to-large scale generator will be made on the basis of technical implementation problems and of other indexes like construction costs and generated power density with respect to land occupation. Experimental data, collected using the small-scale KiteGen prototype built at Politecnico di Torino, are compared to simulation results. The good matching between simulation and real measured data increases the confidence with the presented simulation results, which show that energy generation with controlled power kites can represent a quantum leap in wind power technology, promising to obtain renewable energy from a source largely available almost everywhere, with production costs lower than those of fossil sources.

Index Terms—Constrained control, nonlinear systems, predictive control, renewable energy, wind energy.

I. INTRODUCTION

GLOBAL wind power has the potential to meet the world's energy demand and, differently from fossil sources, it is largely available almost everywhere (see, e.g., [1]). However, the actual wind power technology, based on wind towers, has several limitations that need to be overcome to make such energy source competitive against fossil sources (for an overview of the present wind technology, see, e.g., [2]). In particular, wind

Manuscript received April 24, 2008; revised September 29, 2008 and November 17, 2008. Manuscript received in final form March 10, 2009. Recommended by Associate Editor M. L. Corradini. This work was supported in part by funds of Ministero dell'Istruzione dell'Università e della Ricerca of Italy, under the National Project "Advanced control and identification techniques for innovative applications", and by funds of Regione Piemonte, Italy, under the Projects "Controllo di aquiloni di potenza per la generazione eolica di energia" and "KiteNav: power kites for naval propulsion".

The authors are with the Dipartimento di Automatica e Informatica, Politecnico di Torino, Corso Duca degli Abruzzi 24-10129 Torino, Italy (e-mail: massimo.canale@polito.it; lorenzo.fagiano@polito.it; mario.milanese@polito.it).

Digital Object Identifier 10.1109/TCST.2009.2017933

towers require heavy foundations and huge blades, with massive investments leading to higher energy production costs with respect to thermal plants. Moreover, the average power density per km^2 obtained by the present wind farms is 200–300 times lower than that of big thermal plants of the same rated power, leading to significant land occupation and impact on the environment. Finally, wind towers can operate at a maximum height of about 150 m, due to structural limits, and can therefore be used with profit only in locations with "good" wind speed at 50–150 m of height from the ground.

Recent studies (see, e.g., [3]–[6] and [7]) have shown that these limitations can be overcome by the developing technology of high altitude wind power. The basic idea is to capture wind energy using tethered airfoils (e.g., power kites used for surfing or sailing) whose flight is suitably driven by an automatic control unit. Wind energy is collected at ground level by converting the mechanical power transferred by the kite lines into electrical power, using a suitable mechanism and electric generators. This class of power generators, which will be referred to as "KiteGen" in the following, are able to exploit wind flows at higher altitudes (up to 1000 m), where quite strong and constant wind can be found basically everywhere in the world. Thus, this technology can be used in a much larger number of locations. Moreover, the strength of high altitude wind flows can be more effectively exploited, since the generated power grows with the cube of wind speed, leading to higher power values with respect to those of wind towers placed in the same location. Furthermore, the bulky structure of a KiteGen is kept at ground level, while only airfoils and their lines move in the air: thus, the construction costs of this kind of generator are much lower than those of a wind mill of the same rated power (i.e., the level for which the electrical system has been designed, see [2]), since the structural problems, given in wind towers by unbalanced forces and masses at the tower's hub, are avoided by the system architecture in a KiteGen. Finally, also from the point of view of system safety the KiteGen shows quite big advantages, since the physical and economical damage given by the breaking of a kite or a line would be much lower than those given by the breaking of a wind tower. Due to all these reasons, it is expected that a KiteGen will have a generated power density per kilometers squared much higher than a wind farm and much lower energy production costs, even lower than fossil energy.

In this paper, new simulation results and experimental data are given, related to the KiteGen project undergoing at Politecnico di Torino. Two different kinds of KiteGen have been investigated so far in the project (see [3]–[5]): the *yo-yo configuration* and the *carousel configuration*. In both these configurations, the kite lines are rolled around two drums, linked to two electric drives able to act either as generators or as motors, and

the control system can influence the kite motion by differentially pulling the lines (see Section III). The system composed by the electric drives, the drums, and all the hardware needed to control a single kite will be denoted as Kite Steering Unit (K.S.U.) and it represents the core of the KiteGen. In the yo-yo configuration, wind power is captured by unrolling the kite lines, while in the carousel configuration the K.S.U. is also employed to drag a vehicle moving along a circular rail path, thus generating energy by means of additional electric generators linked to the wheels.

The simulation results obtained with yo-yo and carousel generators are presented here, using a more realistic model for the kite and the lines with respect to the ones used in [3]–[5]. In particular, the improved kite model includes a variable attack angle and, consequently, aerodynamic lift and drag coefficients, derived on the basis of computational fluid dynamics (CFD) analysis. The new line model includes line weight and aerodynamic drag. The simulations presented in this paper have been performed with the same conditions of nominal wind speed and kite area for both the yo-yo and the carousel configurations. Moreover, a new carousel control strategy, with respect to the ones presented in [4] and [5], is considered, in which the line unrolling is exploited to generate energy when the kite is dragged by the carousel against the wind. This way, the overall power, given by the sum of the effects of line rolling/unrolling and carousel motion, is always positive (i.e., generated power) and its course is less variable during each carousel cycle.

The numerical simulations are also employed in this paper to investigate the scalability of the KiteGen technology, in order to make a comparison with the actual wind energy technology. As a second contribution of this paper, experimental data obtained with a yo-yo prototype built at Politecnico di Torino are also presented, which show the good matching between the obtained simulated and real generated power values. This comparison increases the confidence with the presented simulation results. Note that, though the prototype has small maximum peak power (40 kW), it allowed to capture wind energy up to 500–700 m over the ground.

As regards the control strategies, in both the considered KiteGen configurations a single K.S.U. is employed to control the kite flight to generate energy by continuously performing a cycle composed by two phases. In each working phase, the controller design can be formulated as an optimization problem with its own cost function, aimed to maximize the overall generated power, and with state and input constraints, since for example the kite height on the ground cannot be negative and control actuators have their own physical limits. From this point of view, nonlinear model predictive control (MPC) appears to be an appropriate technique to be employed. However, an efficient implementation is needed for the real time control computations at the required sampling time (of the order of 0.2 s): thus, a fast implementation technique of the obtained predictive controller, denoted as FMPC (see [8] and [9]), is used.

This paper is organized as follows. In Section II the considered configurations of kite generators are reviewed and their working phases are explained. The mathematical models used to simulate and control the system are described in Section III,

while MPC design is treated in Section IV. Simulation results with the considered kite generators are reported in Section V; Section VI contains the experimental results obtained with the yo-yo prototype and their comparison with simulation results. Finally, conclusions and further lines of development are reported in Section VII.

II. KITE GENERATORS

A. Yo-Yo Configuration

As a first step, in the KiteGen project a small scale prototype of the yo-yo kite generator has been realized [see Fig. 1(a)]. In this configuration, the K.S.U. is fixed with respect to the ground. Energy is obtained by continuously performing a two-phase cycle [depicted in Fig. 1(b)]: in the *traction phase* the kite exploits wind power to unroll the lines and the electric drives act as generators, driven by the rotation of the drums. When the maximum line length is reached, the *passive phase* begins and the drives act as motors, spending a minimum amount of the previously generated energy, to recover the kite and to drive it in a position which is suitable to start another traction phase, i.e., when the kite is flying with wind advantage in a symmetric zone with respect to the nominal wind direction. As introduced in Section I, two different MPC controllers are designed to control the kite in the traction and passive phases. For the whole cycle to be generative, the total amount of energy produced in the first phase has to be greater than the energy spent in the second one, therefore the controller employed in the traction phase must maximize the produced energy, while the passive phase controller objective is to maneuver the kite in a suitable position while minimizing the energy spent. The yo-yo configuration has been studied in [3] and [4], considering a very simple system model that did not take into account the line weight and drag and variable kite aerodynamic coefficients. The potential of the yo-yo configuration has also been investigated in [10] for the cases of one and two kites linked to a single cable: optimal kite periodic loops, which maximize the generated energy, are computed considering as inputs the derivatives of the kite roll angle and lift coefficient and of the cable winding speed. Moreover, in [6] a real time nonlinear MPC scheme is used to control a single kite and make it track precomputed optimal reference orbits which are parameterized with respect to the nominal wind speed. In this paper, no precomputed orbit is used and the designed nonlinear MPC controller directly maximizes the generated energy. Moreover, the employed sampling time of 0.2 s is quite lower than the value used in [6] (equal to 1 s) and the kite lift coefficient is not an input variable. The latter difference is due to the presence of a different kind of actuator: in the yo-yo prototype built at Politecnico di Torino, which this paper refers to, the kite is commanded just by differentially pulling its two lines, while in the prototype built at Delft University (see e.g., [7]), which [6] refers to, wireless-commanded linear actuators are put on the kite lateral extremes, to make it possible to also change its attack angle (i.e., the aerodynamic characteristics), by changing the position of the line attach points on each side of the kite.

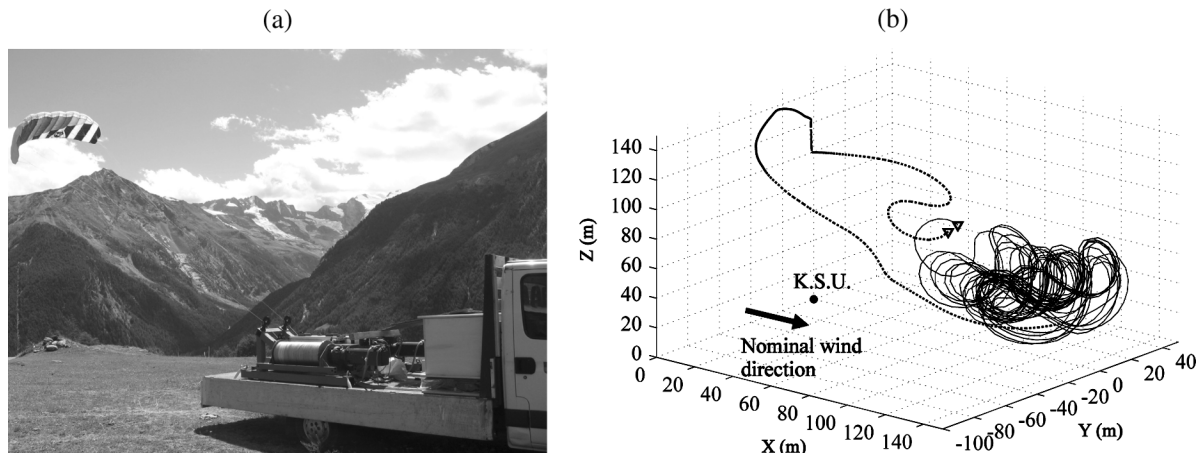


Fig. 1. (a) KiteGen small scale prototype of yo-yo configuration. (b) Yo-yo configuration cycle: traction (solid line) and passive (dashed line) phases.

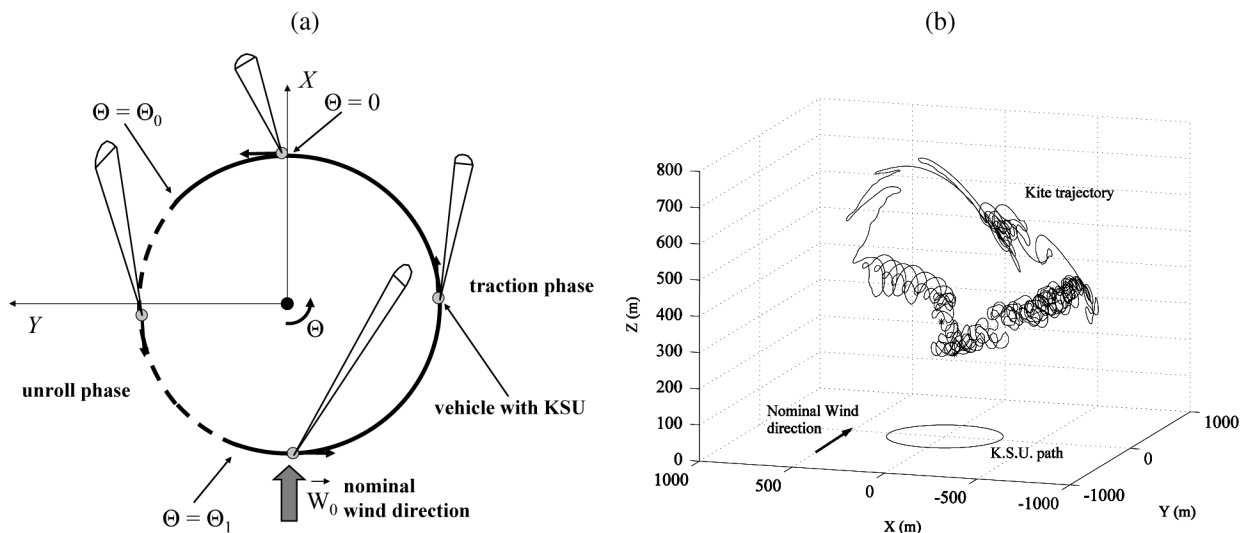


Fig. 2. (a) Carousel configuration phases. (b) Kite and K.S.U. trajectories during a cycle with carousel configuration.

B. Carousel Configuration

In such a configuration, several airfoils are controlled by their K.S.U.s placed on vehicles moving along a circular rail path; the speeds of such vehicles are kept constant by electric generators/motors acting on the wheels. The potentials of the KiteGen carousel configuration have been investigated in [4], where varying line length was considered, and in [5], where the length of the lines was kept constant during the carousel cycle. In both these previous studies, the same simple kite model of [3] was considered and a cycle composed of two phases was used: in the first phase the kite pulled the carousel, thus generating energy, while in the second phase the kite was dragged against the wind and driven in a position such that the energy loss was much lower than the amount previously produced.

In this paper, a new control strategy for the carousel configuration is introduced, able to generate energy also when the rail vehicle is moving against the wind. The operating phases of each kite steering unit (K.S.U.) placed on the carousel are depicted in Fig. 2(a)–(b). The *unroll phase* approximately be-

gins when the angular position Θ of the rail vehicle is such that the K.S.U. is moving in the opposite direction with respect to the nominal wind: such situation is identified by angle Θ_0 in Fig. 2(a). During the unroll phase, the electric drives linked to the rail vehicle wheels act as motors to drag the K.S.U. against the wind. At the same time, the kite lines unroll, thus energy is generated as in the traction phase of the yo-yo configuration. The difference between the energy spent to drag the rail vehicle and the energy generated by unrolling the lines gives the net energy generated during this phase. When the K.S.U. starts moving with wind advantage [i.e., its angular position is greater than Θ_1 in Fig. 2(a)], the carousel *traction phase* starts: the kite pulls the rail vehicle and the drives linked to the wheels act as generators. Meanwhile, the kite lines are rolled back in order to always start the next unroll phase with the same line length. Thus, in the traction phase the net generated energy is given by the difference between the energy generated by pulling the rail vehicle and the energy spent to recover the lines. The MPC controllers employed in the carousel phases are therefore designed to maximize such a net generated energy. With this new carousel control strategy the overall power, given by the sum of

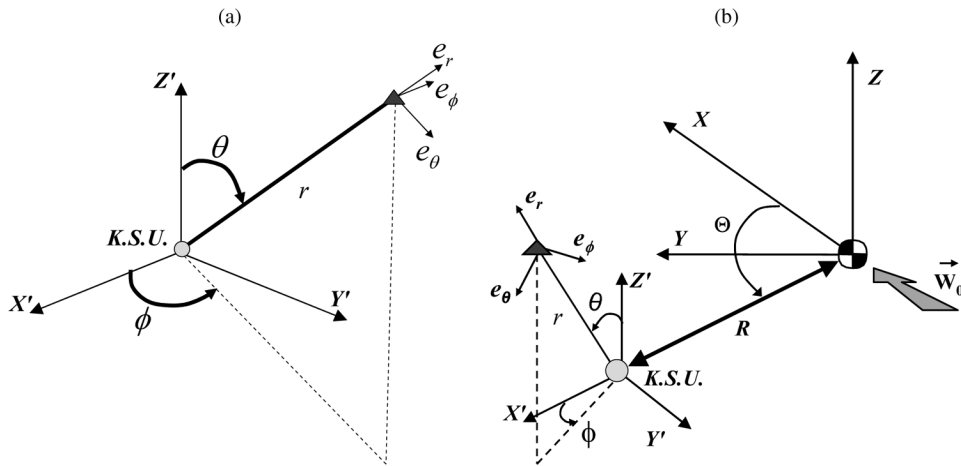


Fig. 3. (a) Model diagram of a single K.S.U. (b) Model diagram of a single K.S.U. moving on a carousel.

the effects of line rolling/unrolling and carousel motion, is always positive (i.e., generated power) and its course is less variable during each cycle.

III. KITE GENERATOR MODELS

A fixed Cartesian coordinate system (X, Y, Z) is considered [see Fig. 3(b)], with X -axis aligned with the nominal wind speed vector direction. Wind speed vector is represented as $\vec{W}_l = \vec{W}_0 + \vec{W}_t$, where \vec{W}_0 is the nominal wind, supposed to be known and expressed in (X, Y, Z) as

$$\vec{W}_0 = \begin{pmatrix} W_x(Z) \\ 0 \\ 0 \end{pmatrix}. \quad (1)$$

$W_x(Z)$ is a known function which gives the wind nominal speed at the altitude Z . The term \vec{W}_t may have components in all directions and is not supposed to be known, accounting for wind unmeasured turbulence.

A second, possibly moving, Cartesian coordinate system (X', Y', Z') is considered, centered at the K.S.U. location. In this system, the kite position can be expressed as a function of its distance r from the origin and of the two angles θ and ϕ , as depicted in Fig. 3(a), which also shows the three unit vectors e_θ , e_ϕ , and e_r of a local coordinate system centered at the kite center of gravity. Unit vectors (e_θ, e_ϕ, e_r) are expressed in the moving Cartesian system (X', Y', Z') by

$$\begin{pmatrix} e_\theta & e_\phi & e_r \end{pmatrix} = \begin{pmatrix} \cos(\theta) \cos(\phi) & -\sin(\phi) & \sin(\theta) \cos(\phi) \\ \cos(\theta) \sin(\phi) & \cos(\phi) & \sin(\theta) \sin(\phi) \\ -\sin(\theta) & 0 & \cos(\theta) \end{pmatrix}. \quad (2)$$

In the carousel configuration, the K.S.U. angular position Θ is defined by the direction of X and X' -axes [see Fig. 3(b)]. Applying Newton's laws of motion to the kite in the local coordinate system (e_θ, e_ϕ, e_r) , the following dynamic equations are obtained:

$$\ddot{\theta} = \frac{F_\theta}{mr}$$

$$\begin{aligned} \ddot{\phi} &= \frac{F_\phi}{mr \sin \theta} \\ \ddot{r} &= \frac{F_r}{m} \end{aligned} \quad (3)$$

where m is the kite mass. Forces F_θ , F_ϕ and F_r include the contributions of gravity force \vec{F}^{grav} of the kite and the lines, apparent force \vec{F}^{app} , kite aerodynamic force \vec{F}^{aer} , aerodynamic drag force $\vec{F}^{\text{c,aer}}$ of the lines and traction force $F^{\text{c,trc}}$ exerted by the lines on the kite. Their relations, expressed in the local coordinates (e_θ, e_ϕ, e_r) are given by

$$\begin{aligned} F_\theta &= F_\theta^{\text{grav}} + F_\theta^{\text{app}} + F_\theta^{\text{aer}} + F_\theta^{\text{c,aer}} \\ F_\phi &= F_\phi^{\text{grav}} + F_\phi^{\text{app}} + F_\phi^{\text{aer}} + F_\phi^{\text{c,aer}} \\ F_r &= F_r^{\text{grav}} + F_r^{\text{app}} + F_r^{\text{aer}} + F_r^{\text{c,aer}} - F^{\text{c,trc}}. \end{aligned} \quad (4)$$

The following subsections describe how each force contribution is taken into account in the model.

A. Gravity Forces

The magnitude of the overall gravity force applied to the kite center of gravity is the sum of the kite weight and the contribution $F^{\text{c,grav}}$ given by the weight of the lines. Assuming that the weight of each line is applied at half its length (i.e., $r/2$), $F^{\text{c,grav}}$ can be computed considering the rotation equilibrium equation around the point where the lines are attached to the K.S.U.

$$\frac{r \cos(\theta)}{2} \frac{2\rho_l \pi d_l^2 r}{4} g = F^{\text{c,grav}} r \cos(\theta) \quad (5)$$

where g is the gravity acceleration, ρ_l is the line material density and d_l is the diameter of each line. Thus, the magnitude of the overall gravity force \vec{F}^{grav} can be computed as

$$|\vec{F}^{\text{grav}}| = mg + F^{\text{c,grav}} = \left(m + \frac{\rho_l \pi d_l^2 r}{4} \right) g. \quad (6)$$

Vector \vec{F}^{grav} in the fixed coordinate system (X, Y, Z) is directed along the negative Z direction. Thus, using the rotation matrix (2) the following expression is obtained for the components of \vec{F}^{grav} in the local coordinates (e_θ, e_ϕ, e_r)

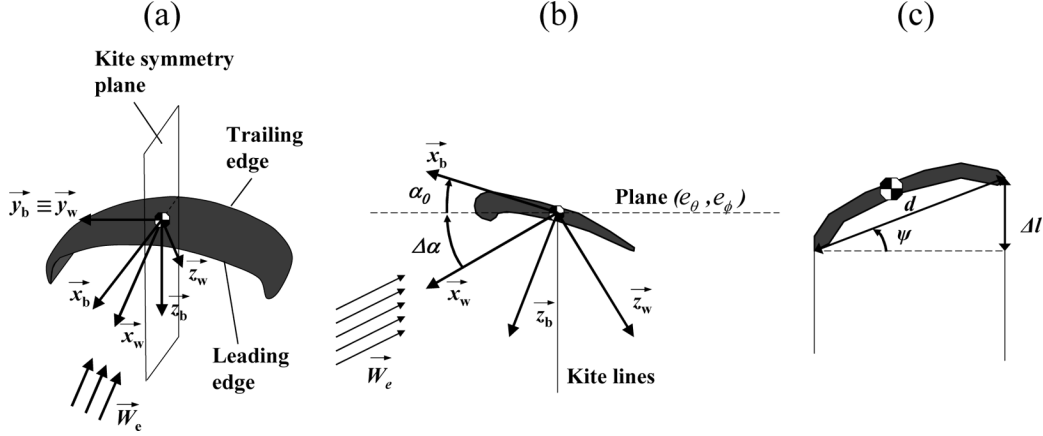


Fig. 4. (a) Scheme of the kite wind coordinate system $(\vec{x}_w, \vec{y}_w, \vec{z}_w)$ and body coordinate system $(\vec{x}_b, \vec{y}_b, \vec{z}_b)$. (b) Wind axes (\vec{x}_w, \vec{z}_w) , body axes (\vec{x}_b, \vec{z}_b) , and angles α_0 and $\Delta\alpha$. (c) Command angle ψ .

$$\vec{F}^{\text{grav}} = \begin{pmatrix} F_\theta^{\text{grav}} \\ F_\phi^{\text{grav}} \\ F_r^{\text{grav}} \end{pmatrix} = \begin{pmatrix} \left(m + \frac{\rho l \pi d^2 r}{4}\right) g \sin(\theta) \\ 0 \\ -\left(m + \frac{\rho l \pi d^2 r}{4}\right) g \cos(\theta) \end{pmatrix}. \quad (7)$$

$$\vec{W}_a = \begin{pmatrix} \dot{\theta} r \\ \dot{\phi} r \sin \theta \\ \dot{r} \end{pmatrix} \quad (11)$$

B. Apparent Forces

The components of vector \vec{F}^{app} depend on the considered kite generator configuration: in particular, for the yo-yo configuration centrifugal inertial forces have to be considered

$$\begin{aligned} F_\theta^{\text{app}} &= m(\dot{\phi}^2 r \sin \theta \cos \theta - 2\dot{r}\dot{\theta}) \\ F_\phi^{\text{app}} &= m(-2\dot{r}\dot{\phi} \sin \theta - 2\dot{\phi}\dot{\theta} r \cos \theta) \\ F_r^{\text{app}} &= m(r\dot{\theta}^2 + r\dot{\phi}^2 \sin^2 \theta). \end{aligned} \quad (8)$$

In the case of carousel configuration, since each K.S.U. moves along a circular trajectory with constant radius R [see Fig. 3(b)], also the effects of the K.S.U. angular position Θ and its derivatives have to be taken into account in apparent force calculation, therefore

$$\begin{aligned} F_\theta^{\text{app}} &= m(\dot{\Theta}^2 R \cos \theta \cos \phi - \ddot{\Theta} R \cos \theta \sin \phi \\ &\quad + (\dot{\Theta} + \dot{\phi})^2 r \sin \theta \cos \theta - 2\dot{r}\dot{\theta}) \\ F_\phi^{\text{app}} &= m(-2\dot{r}\dot{\phi} + \ddot{r}) \sin \theta \\ &\quad - 2(\dot{\Theta} + \dot{\phi})\dot{\theta} r \cos \theta - \ddot{\Theta} R \cos \phi - \dot{\Theta}^2 R \sin \phi) \\ F_r^{\text{app}} &= m(r\dot{\theta}^2 + r(\dot{\Theta} + \dot{\phi})^2 \sin^2 \theta - \ddot{\Theta} R \sin \theta \sin \phi \\ &\quad + \dot{\Theta}^2 R \sin \theta \cos \phi). \end{aligned} \quad (9)$$

C. Kite Aerodynamic Forces

Aerodynamic force \vec{F}^{aer} depends on the effective wind speed \vec{W}_e , which in the local system (e_θ, e_ϕ, e_r) is computed as

$$\vec{W}_e = \vec{W}_l - \vec{W}_a \quad (10)$$

where \vec{W}_a is the kite speed with respect to the ground. For the yo-yo configuration \vec{W}_a can be expressed in the local coordinate system (e_θ, e_ϕ, e_r) as

while for the carousel configuration

$$\vec{W}_a = \begin{pmatrix} \dot{\theta} r + \dot{\Theta} \cos \theta \sin \phi R \\ (\dot{\phi} + \dot{\Theta}) r \sin \theta + \dot{\Theta} \cos \phi R \\ \dot{r} + \dot{\Theta} \sin \theta \sin \phi R \end{pmatrix}. \quad (12)$$

Let us consider now the kite wind coordinate system $(\vec{x}_w, \vec{y}_w, \vec{z}_w)$ [see Fig. 4(a)–(b)], with the origin in the kite center of gravity, \vec{x}_w basis vector aligned with the effective wind speed vector, pointing from the trailing edge to the leading edge of the kite, \vec{z}_w basis vector contained in the kite symmetry plane and pointing from the top surface of the kite to the bottom and wind \vec{y}_w basis vector completing the right-handed system. Unit vector \vec{x}_w can be expressed in the local coordinate system (e_θ, e_ϕ, e_r) as

$$\vec{x}_w = -\frac{\vec{W}_e}{|\vec{W}_e|}. \quad (13)$$

According to [11], vector \vec{y}_w can be expressed in the local coordinate system (e_θ, e_ϕ, e_r) as

$$\vec{y}_w = e_w(-\cos(\psi) \sin(\eta)) + (e_r \times e_w)(\cos(\psi) \cos(\eta)) + e_r \sin(\psi) \quad (14)$$

where

$$\begin{aligned} e_w &= \frac{\vec{W}_e - e_r(e_r \cdot \vec{W}_e)}{|\vec{W}_e - e_r(e_r \cdot \vec{W}_e)|} \\ \eta &= \arcsin\left(\frac{\vec{W}_e \cdot e_r}{|\vec{W}_e - e_r(e_r \cdot \vec{W}_e)|} \tan(\psi)\right). \end{aligned} \quad (15)$$

Angle ψ is the control input, defined by

$$\psi = \arcsin\left(\frac{\Delta l}{d}\right) \quad (16)$$

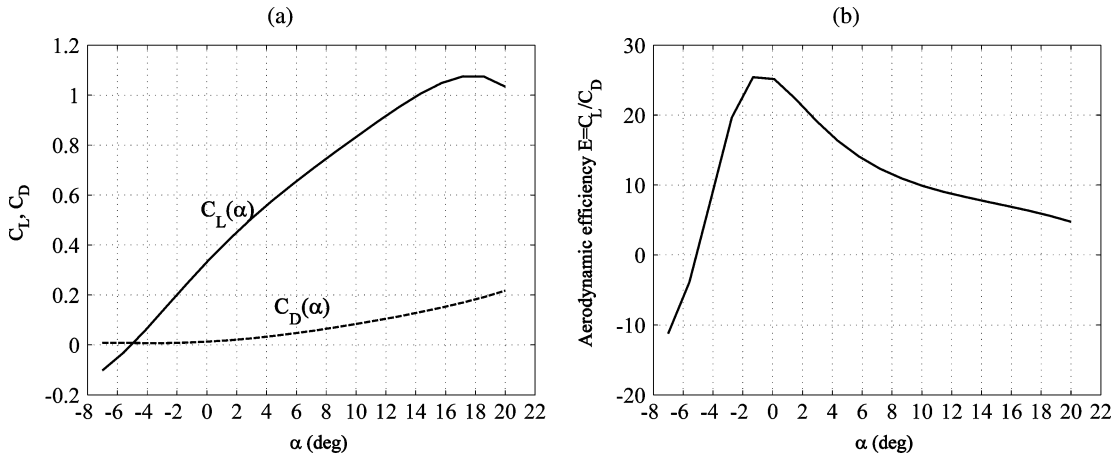


Fig. 5. (a) Kite Lift coefficient C_L (solid line) and drag coefficient C_D (dashed line) as functions of the attack angle α . (b) Aerodynamic efficiency E as function of the attack angle α .

with d being the distance between the two lines fixing points at the kite and Δl the length difference of the two lines [see Fig. 4(b)]. Δl is considered positive if, looking the kite from behind, the right line is longer than the left one. Equation (14) has been derived in [11] in order to satisfy the requirements that \vec{y}_w is perpendicular to \vec{x}_w , that its projection on the unit vector e_r is $\vec{y}_w \cdot e_r = \sin(\psi)$ and that the kite is always in the same orientation with respect to the lines. Angle ψ influences the kite motion by changing the direction of vector \vec{F}^{aer} . Finally, the wind unit vector \vec{z}_w can be computed as

$$\vec{z}_w = \vec{x}_w \times \vec{y}_w. \quad (17)$$

Then, the aerodynamic force \vec{F}^{aer} in the local coordinate system (e_θ, e_ϕ, e_r) is given by

$$\vec{F}^{\text{aer}} = \begin{pmatrix} F_\theta^{\text{aer}} \\ F_\phi^{\text{aer}} \\ F_r^{\text{aer}} \end{pmatrix} = -\frac{1}{2}C_D A \rho |\vec{W}_e|^2 \vec{x}_w - \frac{1}{2}C_L A \rho |\vec{W}_e|^2 \vec{z}_w \quad (18)$$

where ρ is the air density, A is the kite characteristic area, C_L and C_D are the kite lift and drag coefficients. As a first approximation, the drag and lift coefficients are nonlinear functions of the kite angle of attack α . To define angle α , the kite body coordinate system $(\vec{x}_b, \vec{y}_b, \vec{z}_b)$ needs to be introduced [see Fig. 4(a)–(b)], centered in the kite center of gravity with unit vector \vec{x}_b contained in the kite symmetry plane, pointing from the trailing edge to the leading edge of the kite, unit vector \vec{z}_b perpendicular to the kite surface and pointing down and unit vector \vec{y}_b completing a right-handed coordinate system. Such a system is fixed with respect to the kite. The attack angle α is then defined as the angle between the wind axis \vec{x}_w and the body axis \vec{x}_b [see Fig. 4(a)]. Note that in the employed model, it is supposed that the wind axis \vec{x}_w is always contained in the kite symmetry plane. Moreover, it is considered that by suitably regulating the attack points of the lines to the kite, it is possible to impose a desired *base* angle of attack α_0 to the kite: such an angle [depicted in Fig. 4(a)] is defined as the angle between the kite body axis \vec{x}_b and the plane defined by local vectors e_θ and e_ϕ , i.e., the tangent plane to a sphere with radius r . Then, the actual kite angle of attack α can be computed as the sum of α_0

and the angle $\Delta\alpha$ between the effective wind \vec{W}_e and the plane defined by (e_θ, e_ϕ)

$$\alpha = \alpha_0 + \Delta\alpha$$

$$\Delta\alpha = \arcsin\left(\frac{e_r \cdot \vec{W}_e}{|\vec{W}_e|}\right). \quad (19)$$

Functions $C_L(\alpha)$ and $C_D(\alpha)$ employed in this paper are reported in Fig. 5(a), while the related aerodynamic efficiency $E(\alpha) = C_L(\alpha)/C_D(\alpha)$ is reported in Fig. 5(b). Such curves refer to a Clark-Y kite with aspect ratio (i.e., length of leading edge divided by kite width) equal to 3.19 (see Fig. 6) and they have been obtained using CFD analysis with the STAR-CCM+® code (see [12]).

D. Line Forces

The lines influence the kite motion through their weight (see Section III-A), their drag force $\vec{F}^{\text{c,aer}}$ and the traction force $F^{\text{c,trc}}$. An estimate of the drag of the lines has been considered in [10], where the overall angular momentum $\vec{M}_d = r e_r \times \vec{F}^{\text{c,aer}}$ exerted by the line drag force is computed by integrating, along the line length, the angular momentum given by the drag force acting on an infinitely small line segment

$$\vec{M}_d = \int_0^r \left(s e_r \times -\frac{\rho C_{D,l} d_l \cos(\Delta\alpha)}{2} \left(\frac{s |\vec{W}_e|}{r}\right)^2 \vec{x}_w \right) ds$$

$$= r e_r \times -\frac{\rho C_{D,l} A_l \cos(\Delta\alpha)}{8} |\vec{W}_e|^2 \vec{x}_w \quad (20)$$

where $C_{D,l}$ is the line drag coefficient and $A_l \cos(\Delta\alpha) = r d_l \cos(\Delta\alpha)$ is the projection of the line front area on the plane perpendicular to the effective wind vector (see Fig. 7). Note that in [10] the total front line area $A_l = r d_l$ is considered to compute M_d : such assumption is valid if the effective wind speed vector \vec{W}_e is perpendicular to the kite lines, otherwise it leads to a conservative estimation of the line drag force. The line drag force is then computed as

$$\vec{F}^{\text{c,aer}} = \begin{pmatrix} F_\theta^{\text{c,aer}} \\ F_\phi^{\text{c,aer}} \\ F_r^{\text{c,aer}} \end{pmatrix} = -\frac{\rho C_{D,l} A_l \cos(\Delta\alpha)}{8} |\vec{W}_e|^2 \vec{x}_w. \quad (21)$$

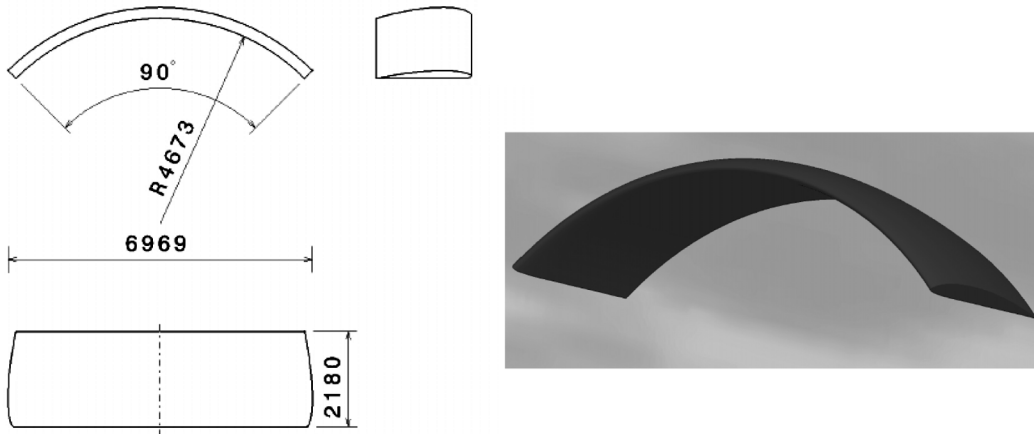


Fig. 6. Geometrical characteristics of the Clark-Y kite considered for the CFD analysis to compute the aerodynamic lift and drag coefficients $C_L(\alpha)$ and $C_D(\alpha)$.

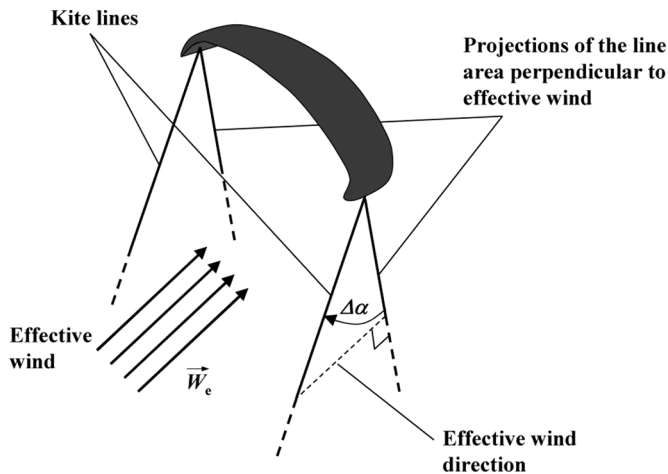


Fig. 7. Detail of the kite lines and their projection on the plane perpendicular to the effective wind vector \vec{W}_e .

The traction force $F^{c, \text{trc}}$ is always directed along the local unit vector e_r and cannot be negative in (4), since the kite can only pull the lines. Moreover, $F^{c, \text{trc}}$ is measured by a force transducer on the K.S.U. and, using a local controller of the electric drives, it is regulated in such a way that $\dot{r}(t) \approx \dot{r}_{\text{ref}}(t)$, where $\dot{r}_{\text{ref}}(t)$ is chosen to achieve a good compromise between high line traction force and high line winding speed. Basically, the stronger the wind, the higher the values of $\dot{r}_{\text{ref}}(t)$ that can be set obtaining high force values. It results that, in the case of yo-yo configuration, $F^{c, \text{trc}}(t) = F^{c, \text{trc}}(\theta, \phi, r, \dot{\theta}, \dot{\phi}, \dot{r}, \dot{r}_{\text{ref}}, \vec{W}_e)$, while for the carousel configuration $F^{c, \text{trc}}(t) = F^{c, \text{trc}}(\theta, \phi, r, \Theta, \dot{\theta}, \dot{\phi}, \dot{r}, \dot{\Theta}, \dot{r}_{\text{ref}}, \vec{W}_e)$.

E. Vehicle Motion in Carousel Configuration

In the case of carousel configuration, the motion law of the K.S.U. along the circular path of radius R has to be included too, with the following equation:

$$M\ddot{\Theta}R = F^{c, \text{trc}} \sin \theta \sin \phi - F^{\text{gen}} \quad (22)$$

where M is the total mass of the rail vehicle and the K.S.U. and F^{gen} is the force given by the electric drives linked to the wheels. It is supposed that suitable kinematic constraints (e.g.,

rails) oppose to the centrifugal inertial force acting on the rail vehicle and to all the components of the line force, except for the one acting along the tangent to the rail vehicle path (i.e., $F^{c, \text{trc}} \sin \theta \sin \phi$). Note that any viscous term is neglected in (22), since the rail vehicle speed $\dot{\Theta}R$ is kept very low as it will be shown in Section V. F^{gen} is positive when the kite is pulling the rail vehicle toward increasing Θ values, thus generating energy, and it is negative when the electric drives are acting as a motors to drag the rail vehicle against the wind, when the kite is not able to generate a suitable pulling force. The force F^{gen} is calculated by a suitable local controller in order to keep the rail vehicle at constant angular speed $\dot{\Theta} = \dot{\Theta}_{\text{ref}}$.

F. Overall Model Equations and Mechanical Power

The model equations (3)–(22) give the system dynamics in the form

$$\dot{x}(t) = f(x(t), u(t), W_x(t), \dot{r}_{\text{ref}}(t), \dot{\Theta}_{\text{ref}}(t), \vec{W}_t(t)) \quad (23)$$

where $x(t) = [\theta(t) \ \phi(t) \ r(t) \ \Theta(t) \ \dot{\theta}(t) \ \dot{\phi}(t) \ \dot{r}(t) \ \dot{\Theta}(t)]^T$ are the model states and $u(t) = \psi(t)$ is the control input. Clearly, in the case of yo-yo configuration $\Theta = \dot{\Theta} = \dot{\Theta}_{\text{ref}} = 0$. All the model states are supposed to be measured or estimated, to be used for feedback control. The net mechanical power P generated (or spent) by the generator is the algebraic sum of the power generated (or spent) by unrolling/recovering the lines and by the rail vehicle movement

$$P(t) = \dot{r}(t)F^{c, \text{trc}}(t) + \dot{\Theta}(t)RF^{\text{gen}}(t). \quad (24)$$

For the yo-yo configuration the term $\dot{\Theta}RF^{\text{gen}} = 0$ and generated mechanical power is only due to line unrolling.

IV. KITE GENERATOR CONTROL

The control problem and related objectives are now described. As highlighted in Section II, the main objective is to generate energy by a suitable control action on the kite. In order to accomplish this aim, a two-phase cycle has been designed for each generator configuration. The two phases are referred to as the *traction phase* and the *passive phase* for the yo-yo and as the *traction phase* and the *unroll phase* for the carousel configuration. A nonlinear Model Predictive Control (MPC,

see, e.g., [13]) strategy is designed for each phase, according to its own cost function, state and input constraints and terminal conditions.

The control move computation is performed at discrete time instants defined on the basis of a suitably chosen sampling period Δ_t . At each sampling time $t_k = k\Delta_t, k \in \mathbb{N}$, the measured values of the state $x(t_k)$ and of the nominal wind speed $W_x(t_k)$ are used to compute the control move through the optimization of a performance index of the form

$$J(U, t_k, T_p) = \int_{t_k}^{t_k+T_p} L(\tilde{x}(\tau), \tilde{u}(\tau), W_x(\tau),) d\tau \quad (25)$$

where $T_p = N_p\Delta_t, N_p \in \mathbb{N}$ is the prediction horizon, $\tilde{x}(\tau)$ is the state predicted inside the prediction horizon according to the state (23), using $\tilde{x}(t_k) = x(t_k)$ and the piecewise constant control input $\tilde{u}(t)$ belonging to the sequence $U = \{\tilde{u}(t)\}, t \in [t_k, t_k+T_p]$ defined as

$$\tilde{u}(t) = \begin{cases} \bar{u}_i, \forall t \in [t_i, t_{i+1}], i = k, \dots, k + T_c - 1 \\ \bar{u}_{k+T_c-1}, \forall t \in [t_i, t_{i+1}], i = k + T_c, \dots, k + T_p - 1 \end{cases} \quad (26)$$

where $T_c = N_c\Delta_t, N_c \in \mathbb{N}, N_c \leq N_p$ is the control horizon. The function $L(\cdot)$ in (25) is suitably defined on the basis of the performances to be achieved in the considered operating phase. Moreover, in order to take into account physical limitations on both the kite behavior and the control input ψ in the different phases, constraints of the form $\tilde{x}(t) \in \mathbb{X}, \tilde{u}(t) \in \mathbb{U}$ have been included too.

Thus the predictive control law is computed using a receding horizon strategy.

- 1) At time instant t_k , get $x(t_k)$.
- 2) Solve the optimization problem

$$\min_U J(U, t_k, T_p) \quad (27a)$$

$$\text{subject to} \quad (27b)$$

$$\tilde{x}(t_k) = x(t_k) \quad (27c)$$

$$\dot{\tilde{x}}(t) = f(\tilde{x}(t), \tilde{u}(t), \dot{r}_{\text{ref}}(t), \dot{\Theta}_{\text{ref}}(t), W_x(t)) \quad (27d)$$

$$\forall t \in (t_k, t_k+T_p]$$

$$\tilde{x}(t) \in \mathbb{X}, \quad \tilde{u}(t) \in \mathbb{U} \quad \forall t \in [t_k, t_k+T_p]. \quad (27e)$$

- 3) Apply the first element of the solution sequence U to the optimization problem as the actual control action $u(t_k) = \tilde{u}(t_k)$.

4) Repeat the whole procedure at the next sampling time t_{k+1} . Therefore, the predictive controller results to be a nonlinear static function of the system state x , the nominal measured wind speed W_x and the reference speed values $\dot{r}_{\text{ref}}, \dot{\Theta}_{\text{ref}}$ imposed to the local drive controllers of the K.S.U. and of the carousel vehicle (see Sections III-D and III-E)

$$\psi(t_k) = \kappa(x(t_k), W_x(t_k), \dot{r}_{\text{ref}}, \dot{\Theta}_{\text{ref}}(t_k)) = \kappa(w(t_k)). \quad (28)$$

As a matter of fact, an efficient NMPC implementation is required to ensure that the control move is computed within the employed sampling time, of the order of 0.2 s. This is obtained using the fast model predictive control (FMPC) techniques introduced and described in [8] and [9], based on set membership

(SM) approximation. Such techniques allow to compute an approximated control law $\kappa^{\text{SM}}(w) \approx \kappa(w)$ with guaranteed performance and stabilizing properties (the interested reader is referred to [8], [9], and [14] for further details).

Cost functions and state and input constraints considered for the yo-yo configuration are reported in [3] and [4], while [4] and [5] describe the previously employed carousel control strategy. The MPC design for the new carousel control strategy considered in this paper is now presented.

A. New Carousel Control Strategy

In the carousel configuration, the force F^{gen} applied by the electric drives to the rail vehicle wheels is such that the vehicle moves at reference angular speed $\dot{\Theta}_{\text{ref}}$, which is kept constant and it is chosen in order to optimize the net energy generated in the cycle. Since the angular speed is constant, each kite placed on the carousel can be controlled independently from the others, provided that their respective trajectories are such that their lines never collide. Thus, a single rail vehicle is considered in the following.

The traction phase begins when the K.S.U. angular position Θ with respect to the nominal wind vector \vec{W}_0 is such that the kite can pull the rail vehicle [see Fig. 2(a)]. Thus, the following traction phase initial condition is considered:

$$\Theta(t) \geq \Theta_1. \quad (29)$$

At the beginning of the traction phase, the line length is equal to a value r_1 resulting from the previous unroll phase (see Section II-B). Thus, a value $\dot{r}_{\text{trc}} < 0$ for reference speed \dot{r}_{ref} is set during the traction phase in order to roll back the lines and begin the next unroll phase with a suitable line length value r_0 . Recalling that mechanical power (24) obtained at each instant is the sum of the effects given by line unrolling and rail vehicle movement, the following cost function is chosen to be minimized in MPC design (27):

$$J(t_k) = - \int_{t_k}^{t_k+T_p} (\dot{r}(\tau)F^{\text{c, trc}}(\tau) + R\dot{\Theta}(\tau)F^{\text{gen}}(\tau))d\tau. \quad (30)$$

The traction phase ends when the K.S.U. angular position Θ is such that the kite is no more longer able to pull the rail vehicle

$$\Theta(t) \geq \Theta_0 \quad (31)$$

with $\Theta_0 \leq \pi/2$ according to Fig. 2(a).

When condition (31) is reached, the unroll phase starts and the electric drives linked to the rail vehicle wheels act as motors to drag the K.S.U. between angles Θ_0 and Θ_1 . Meanwhile, a suitable course of the reference \dot{r}_{ref} is set to make the unrolling speed \dot{r} smoothly reach the positive constant value \dot{r}_c , so that energy can be generated while the K.S.U. moves against the nominal wind flow. During the unroll phase, the line length increases from the starting value r_0 to a final value $r_1 > r_0$. As regards the choice of \dot{r}_c , note that the mechanical power which opposes to the rail vehicle movement due to the line traction force is

$$P_{\text{res}}(t) = |R\dot{\Theta}(t)F^{\text{c, trc}}(t) \sin \theta(t) \sin \phi(t)| \leq |R\dot{\Theta}(t)F^{\text{c, trc}}(t)|. \quad (32)$$

The mechanical power generated by line unrolling is

$$P_{\text{gen}}(t) = |\dot{r}(t)F^{c,\text{trc}}(t)| \quad (33)$$

thus if $\dot{r}(t) > R\dot{\Theta}(t)$ the net mechanical power $P_{\text{gen}}(t) - P_{\text{res}}(t)$ is positive and as a first approximation, without considering friction forces and losses in electric power conversion, energy is generated. Therefore, a good choice for \dot{r}_c would be

$$\dot{r}_c > R\dot{\Theta}_{\text{ref}}. \quad (34)$$

However, the reference unroll speed \dot{r}_c should not be too high in order to keep the final line length r_1 below a reasonable value \bar{r} (i.e., 1000–1200 m). Since $r_1 \simeq r_0 + \dot{r}_c R(\Theta_1 - \Theta_0)/(R\dot{\Theta}_{\text{ref}})$, the following choice is made

$$\dot{r}_c \simeq \frac{\bar{r} - r_0}{(\Theta_1 - \Theta_0)} \dot{\Theta}_{\text{ref}}. \quad (35)$$

The cost function considered in MPC design for the unroll phase is the same as for the traction phase (30), to maximize the net generated energy

$$J(t_k) = - \int_{t_k}^{t_k + T_p} (\dot{r}(\tau)F^{c,\text{trc}}(\tau) + R\dot{\Theta}(\tau)F^{\text{gen}}(\tau)) d\tau. \quad (36)$$

During the whole carousel cycle, the following state constraint is considered to keep the kite sufficiently far from the ground:

$$\theta(t) \leq \bar{\theta} \quad (37)$$

with $\bar{\theta} < \pi/2$ rad. Actuator physical limitations give rise to the constraints

$$|\psi(t)| \leq \bar{\psi} \quad |\dot{\psi}(t)| \leq \bar{\dot{\psi}}. \quad (38)$$

As a matter of fact, other technical constraints have been added to force the kite to go along “figure eight” trajectories rather than circular ones, in order to prevent the lines from wrapping one around the other. Such constraints force the kite ϕ angle to oscillate with double period with respect to θ angle, thus generating the proper kite trajectory.

V. SIMULATION RESULTS

In the presented simulation tests, the nominal wind speed (1) is given as

$$W_x(Z) = \begin{cases} 0.04Z + 8 & \text{if } Z \leq 100 \text{ m} \\ 0.0171(Z - 100) + 12 & \text{if } Z > 100 \text{ m} \end{cases} \text{ m/s}. \quad (39)$$

Nominal wind speed is 8 m/s at 0 m of altitude and grows linearly to 12 m/s at 100 m and up to 24 m/s at 800 m of height. Moreover, uniformly distributed random wind turbulence \vec{W}_t has also been introduced, with maximum absolute value along

TABLE I
YO-YO CONFIGURATION: MODEL AND CONTROL PARAMETERS

m	50	Kite mass (kg)
A	100	Characteristic area (m ²)
d_l	0.025	Diameter of a single line (m)
ρ_l	970	Line density (kg/m ³)
$C_{D,l}$	1	Line drag coefficient
α_0	3.5	Base angle of attack (°)
ρ	1.2	Air density (kg/m ³)
\bar{r}	2	Traction phase reference \dot{r}_{ref} (m/s)
$\underline{\dot{r}}$	-4	Drag phase reference \dot{r}_{ref} (m/s)
T_c	0.2	Sample time (s)
N_c	1	Control horizon (steps)
N_p	10	Prediction horizon (steps)

TABLE II
YO-YO CONFIGURATION: STATE AND INPUT CONSTRAINTS, CYCLE STARTING, AND ENDING CONDITIONS

$\underline{\theta}_I$	35°	Traction phase starting conditions
$\bar{\theta}_I$	75°	
ϕ_I	45°	
r_I	510 m	
\bar{r}_I	530 m	
\bar{r}	1000 m	1 st Passive sub-phase starting condition
ϕ_{II}	45°	2 nd Passive sub-phase starting conditions
$\bar{\theta}_{II}$	20°	
θ	75°	State constraint
ψ	3°	Input constraints
$\dot{\psi}$	20 °/s	

each direction equal to 4 m/s, i.e., 30% of the nominal wind speed at 100 m of altitude.

A. yo-yo Configuration

The results of three complete yo-yo cycles are reported: the related numerical values of model and control parameters introduced in Sections II–IV are reported in Tables I and II.

The variables $\underline{\theta}_I$, $\bar{\theta}_I$, ϕ_I , r_I , \bar{r}_I , \bar{r} , ϕ_{II} , and $\bar{\theta}_{II}$ in Table II define the starting and ending conditions for each phase of the yo-yo working cycle, for further details the interested reader is referred to [3] and [4].

Fig. 8(a) shows the course of the line length, which is kept between 500 and 1000 m. The obtained kite trajectory during a cycle is reported in Fig. 8(b). It can be seen that the kite follows “figure eight” orbits during the traction phase, thus preventing line entangling. The kite height usually goes from 200 to 600 m during the traction phase, corresponding to a mean value of $\theta(t)$ equal to 60°, while the lateral angle $\phi(t)$ oscillates between $\pm 10^\circ$ with zero in average. This means that the kite is flying fast in crosswind direction, maximizing the generated energy. The power generated in the simulation is reported in Fig. 9(a): the mean value is 793 kW. Note that the considered random disturbances do not cause system instability, showing the control system robustness. The course of the wind effective speed magnitude $|\vec{W}_e|$ is reported in Fig. 9(b): mean values of 105 m/s during the traction phase and 40 m/s during the passive phase

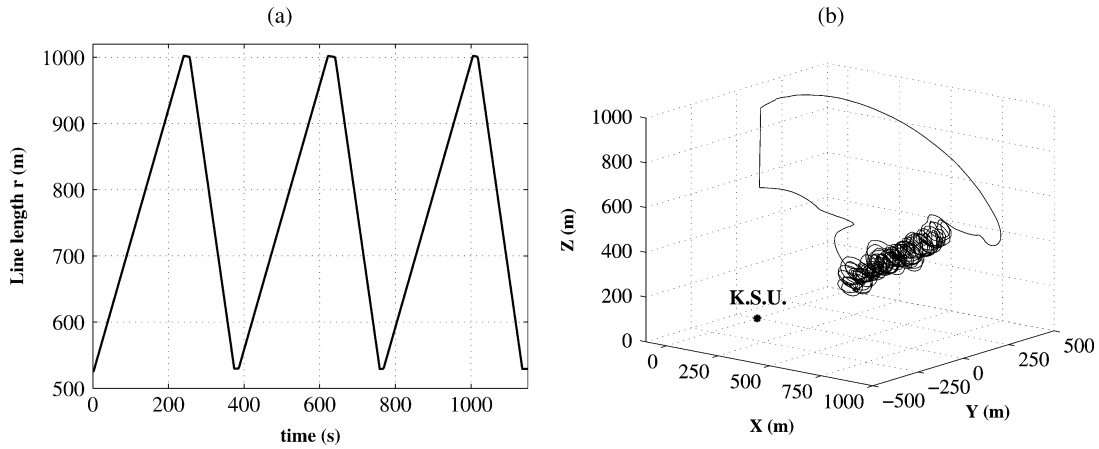


Fig. 8. (a) Line length $r(t)$ during three complete yo-yo cycles with random wind disturbances. (b) Kite trajectory during a yo-yo cycle with random wind disturbance.

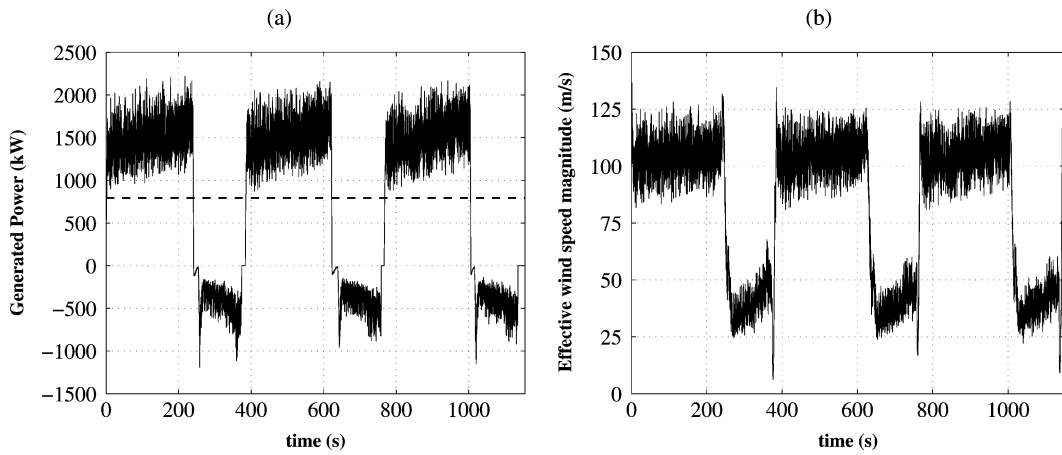


Fig. 9. (a) Mean (dashed line) and actual (solid line) generated power and (b) effective wind speed magnitude $|\vec{V}_e|$ during three complete yo-yo cycles with random wind disturbances.

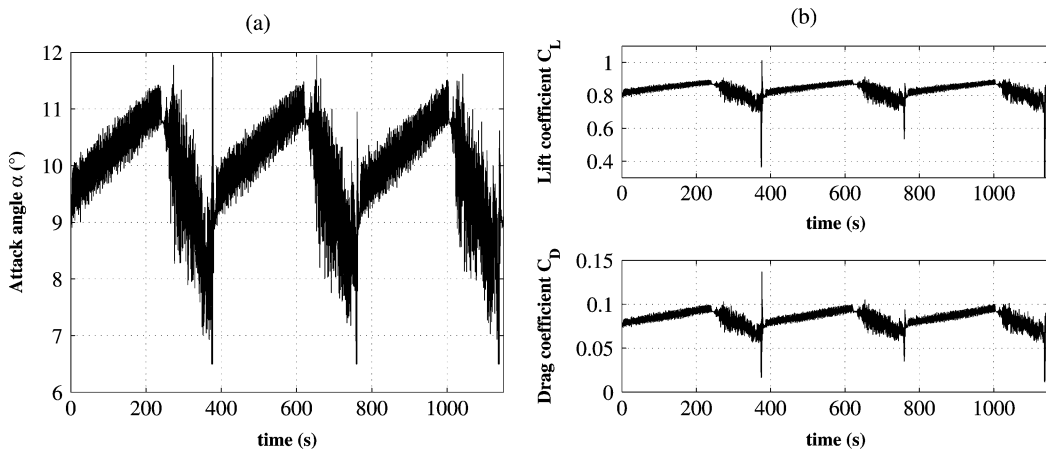


Fig. 10. Kite (a) attack angle and (b) lift and drag coefficients during three yo-yo cycles with random wind disturbances.

are achieved. The obtained kite attack angle and consequent lift and drag coefficients are reported in Fig. 10(a)–(b). The related kite aerodynamic efficiency is between 9 and 12, with a mean value of 10.

B. Carousel Configuration

The considered carousel model and control parameters are given in Table III, while Table IV contains the starting and

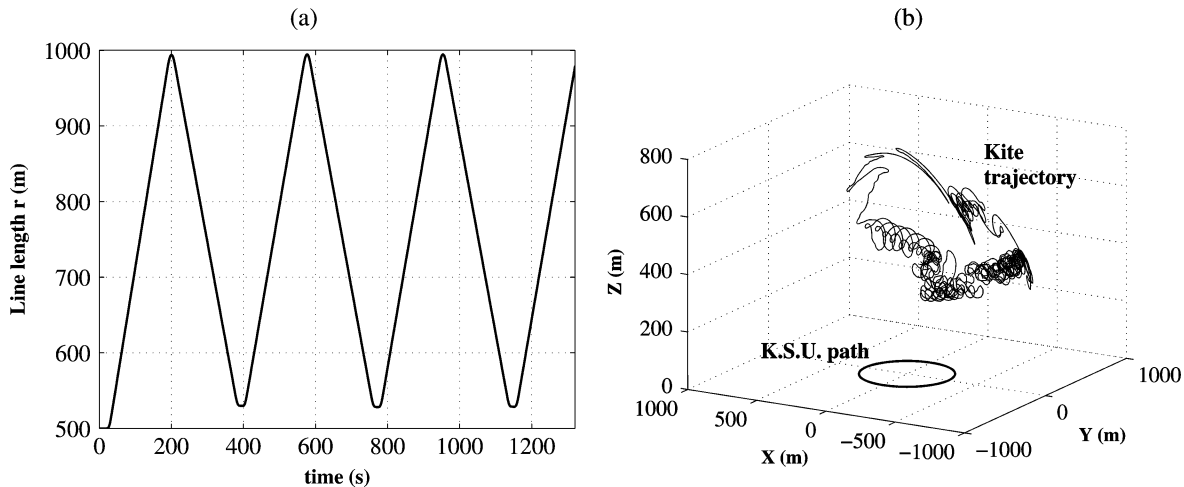


Fig. 11. (a) Line length $r(t)$ during three complete carousel cycles with random wind disturbances. (b) Kite and K.S.U. trajectories during a single carousel cycle with random wind disturbances.

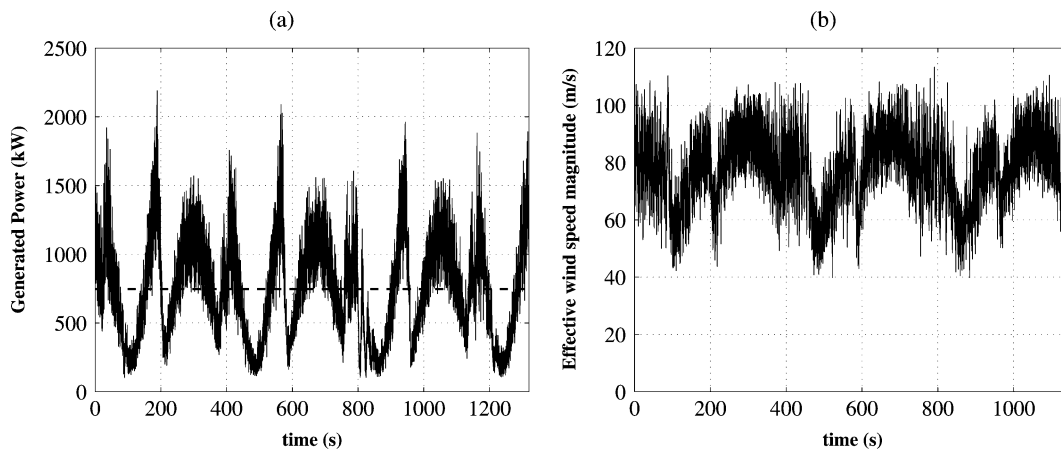


Fig. 12. (a) Mean (dashed line) and actual (solid line) generated power and (b) effective wind speed magnitude $|\vec{W}_e|$ during three complete carousel cycles with random wind disturbances.

ending conditions for each phase, as well as the values of the considered state and input constraints (see Sections II–IV). According to (35), the employed value of \dot{r}_c during the unroll phase is

$$\dot{r}_c = 2.77 \simeq 2.98 = \frac{\bar{r} - r_0}{(\Theta_1 - \Theta_0)} \dot{\Theta}_{\text{ref}}. \quad (40)$$

The obtained course of $r(t)$ is reported in Fig. 11(a). The line length is kept between 500 and 1000 m and its mean value is equal to 747 m. Fig. 11(b) shows the obtained kite and K.S.U. trajectories. The power generated during the two cycles is reported in Fig. 12(a): the mean value is 750 kW. Fig. 12(b) depicts the obtained course of the wind effective speed magnitude $|\vec{W}_e|$. Note that since the fixed coordinate system (X, Y, Z) has been defined on the basis of the nominal wind direction, a measurable change of the latter can be easily overcome by rotating the whole coordinate system (X, Y, Z) , thus obtaining the same performances without changing neither the control system parameters nor the starting conditions of the various phases. Finally, kite attack angle and lift and drag coefficients are reported in Fig. 13(a)–(b). The related aerodynamic efficiency is between 8.7 and 10.2, with a mean value of 9.1.

C. Kite Generator Scalability

To investigate the scalability of the KiteGen technology, numerical simulations have been employed to compute the mean generated power as a function of the kite area, of the kite efficiency, of the mean cable length during the cycle and of wind speed. In all the performed simulations, very similar performances were obtained with the yo-yo and the carousel configurations. The obtained results are showed in Fig. 14. If not differently specified, a kite area of 500 m², with efficiency of 13 and lift coefficient of 1.2, a mean line length of 800 meters, and a constant wind speed of 9 m/s were considered in the simulations. It can be noted that the generated power increases linearly with the kite area, with the cube of wind speed and according to a logistic-type function with the kite aerodynamic efficiency. As regards the dependence on the mean line length, it can be observed that there is an optimal point (which depends on the wind-elevation characteristic $W_x(Z)$) in which the positive effect of higher wind speed values, obtained with longer cables, is counter-balanced by the negative effect of higher cable weight

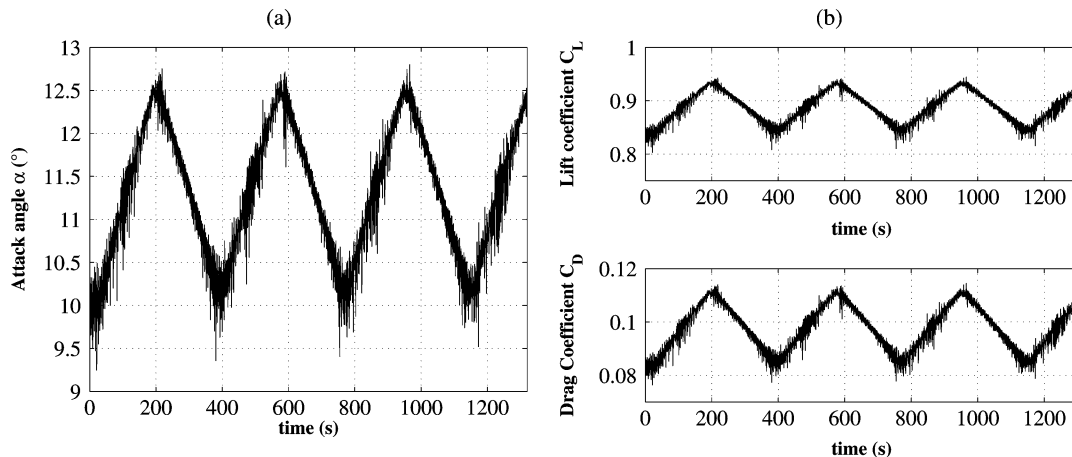


Fig. 13. Kite (a) attack angle and (b) lift and drag coefficients during three carousel cycles with random wind disturbances.

TABLE III
CAROUSEL CONFIGURATION: MODEL AND CONTROL PARAMETERS

m	50	Kite mass (kg)
A	100	Characteristic area (m ²)
M	10000	Vehicle mass (kg)
R	300	Rotor radius (m)
d_l	0.025	Diameter of a single line (m)
ρ_l	970	Line density (kg/m ³)
$C_{D,l}$	1	Line drag coefficient
ρ	1.2	Air density (kg/m ³)
α_0	3.5	Base angle of attack (°)
\dot{r}_c	2.77	Reference line unrolling speed (m/s)
v_{ref}	5	Reference rail vehicle tangential speed (m/s)
T_c	0.2	Sample time (s)
N_c	1	Control horizon (steps)
N_p	12	Prediction horizon (steps)

TABLE IV
CAROUSEL CONFIGURATION: OBJECTIVES AND STARTING CONDITIONS OF THE CYCLE PHASES, STATE, AND INPUT CONSTRAINTS

Θ_0	5°	Unroll phase starting condition
Θ_1	165°	Traction phase starting condition
$\bar{\theta}$	75°	State constraint
ψ	3°	Input constraints
$\dot{\psi}$	20°/s	

and drag force. Beyond this point, an increase of cable length lead to lower mean generated power.

Note that in all the performed simulations the cable diameter has been dimensioned, considering a safety coefficient of 1.2, in accordance with the traction force exerted by the kite, which vary with the different considered parameter values. To this end, the breaking load characteristics of the polyethylene fiber composing the cables, reported in Fig. 15, has been employed.

VI. EXPERIMENTAL TESTS

In this section, experimental data obtained with the small-scale yo-yo prototype built at Politecnico di Torino are showed and compared to simulation results, in order to assess the matching between simulated and real generated energy. Such evaluation is useful to estimate the confidence level in the simulation results reported in Section V. In particular, the measured generated power, line length, and line speed related to two different experimental sessions are reported [see

Fig. 16(a)–(f)]. In both cases, the kite was controlled by a human operator. The collected measured values of line speed have been employed as reference speed to perform a simulation with the model described in Section III. The first data are related to experimental tests performed in Sardinia, Italy, in September 2006, in presence of a quite good (although very disturbed) wind of about 4–5 m/s at ground level. The employed kite had an effective area of 5 m² and the maximum line length was 300 m. Fig. 16(a) and (b) show the comparison between experimental and simulated line length r and line speed \dot{r} . The obtained courses of generated power are reported in Fig. 16(c) and show that good correspondence between simulated and experimental data is achieved. The same analysis has been performed on the data collected in January, 2008, during experimental tests performed at the airport of Casale Monferrato near Torino, Italy. The wind flow was quite weak (1–2 m/s at ground level and about 3–4 m/s at 500 m of height). The employed kite had an effective area of 10 m² and line length of 800 m. The courses of experimental and simulated line length and speed and power values are reported in Fig. 16(d)–(f). Also in this case, a good matching between real measured and simulated data can be observed. Movies of the experimental tests performed near Torino are available on the website [15].

VII. CONCLUSION AND PERSPECTIVES

This paper presented simulation and experimental results regarding a new class of wind energy generators, denoted as KiteGen, which employ tethered airfoils to capture wind power. More realistic models, with respect to previous works, have been used for the kite and its lines and a novel control strategy for the carousel configuration has been introduced too. The presented simulation results show that the power generation potentials of the yo-yo and carousel configurations are very similar. Thus, the choice between these two configurations for further development will be made on the basis of technical implementation problems and of other indexes, like construction costs and generated power density per kilometers squared. The presented experimental data, collected using the small-scale KiteGen prototype built at Politecnico di Torino, have been compared to simulation results. The good matching between

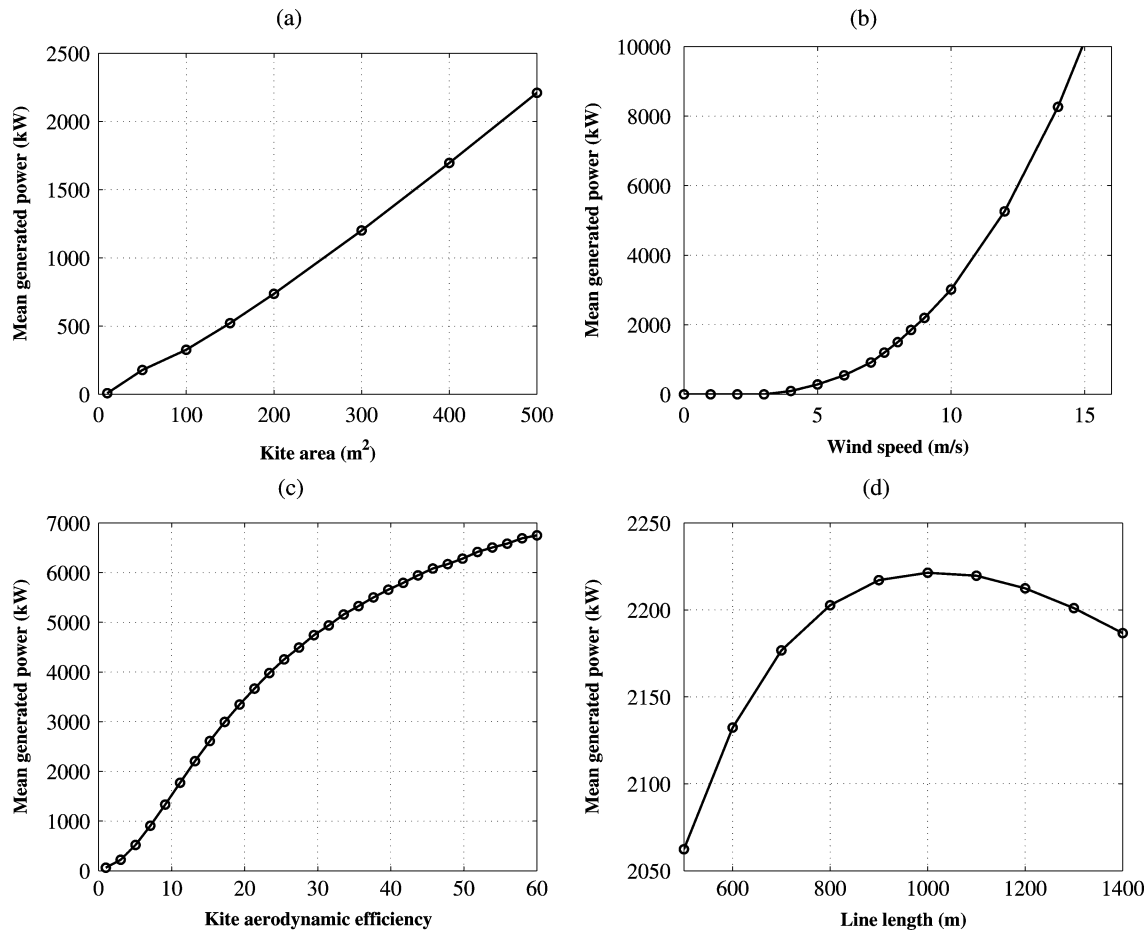


Fig. 14. Mean generated power obtained in the numerical simulations as a function of: (a) kite area; (b) wind speed; (c) aerodynamic efficiency; and (d) line length.

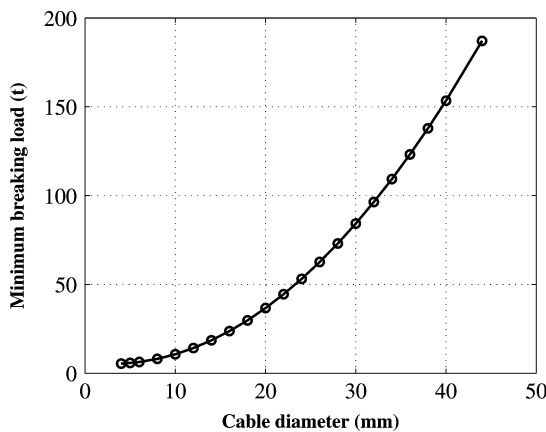


Fig. 15. Breaking load of the cable as a function of its diameter.

simulation and real measured data increases the confidence with the obtained simulation results. The performed study also allowed to investigate the scalability of the KiteGen technology. Such results can be used to make a comparison with the actual wind tower technology. Indeed, it can be noted that a KiteGen generator with a 500-m² kite, with a wind speed of 9 m/s, would be able to produce 2 MW of power, while a present wind tower with 90-m diameter (i.e., 2-MW nominal power with 12-m/s wind) would provide only 1 MW in the

same wind conditions. Moreover, it has to be noted that the rotor and the tower of a wind turbine, whose total weight is between 230 and 330 tons (depending on the tower's height), are replaced in KiteGen by the kite (about 0.5 tons) and its lines (about 2.5 tons for two 1000-m long, 4-cm diameter cables), with reduced construction costs. Finally, according to our preliminary analysis of the wind data contained in the database RAOB (RAwinsonde OBServation) of the National Oceanographic and Atmospheric Administration [16], taking advantage of the higher frequency with which stronger wind is encountered between 200 and 800 meters over the ground, on "good" sites for wind towers the KiteGen technology would have a capacity factor (i.e., the ratio between yearly average power and nominal power) about two times higher than wind towers. Moreover, a KiteGen generator could be employed also in sites where a wind tower would not be profitable, due to weak wind between 0 and 150 m above the ground. The study of KiteGen farms operating with several airfoils, optimizing the number and position of the K.S.U.s and kite trajectories to take into account the problems related to collisions and aerodynamic interference, is currently undergoing. However, according to the first results, the average generated power per kilometers squared of a kite wind farm will be 3–9 times higher than that of an actual wind turbine farm in a "good" site. Thus, even with the conservative assumption that the cost of KiteGen technology is the same of wind towers, an energy cost of 20–50

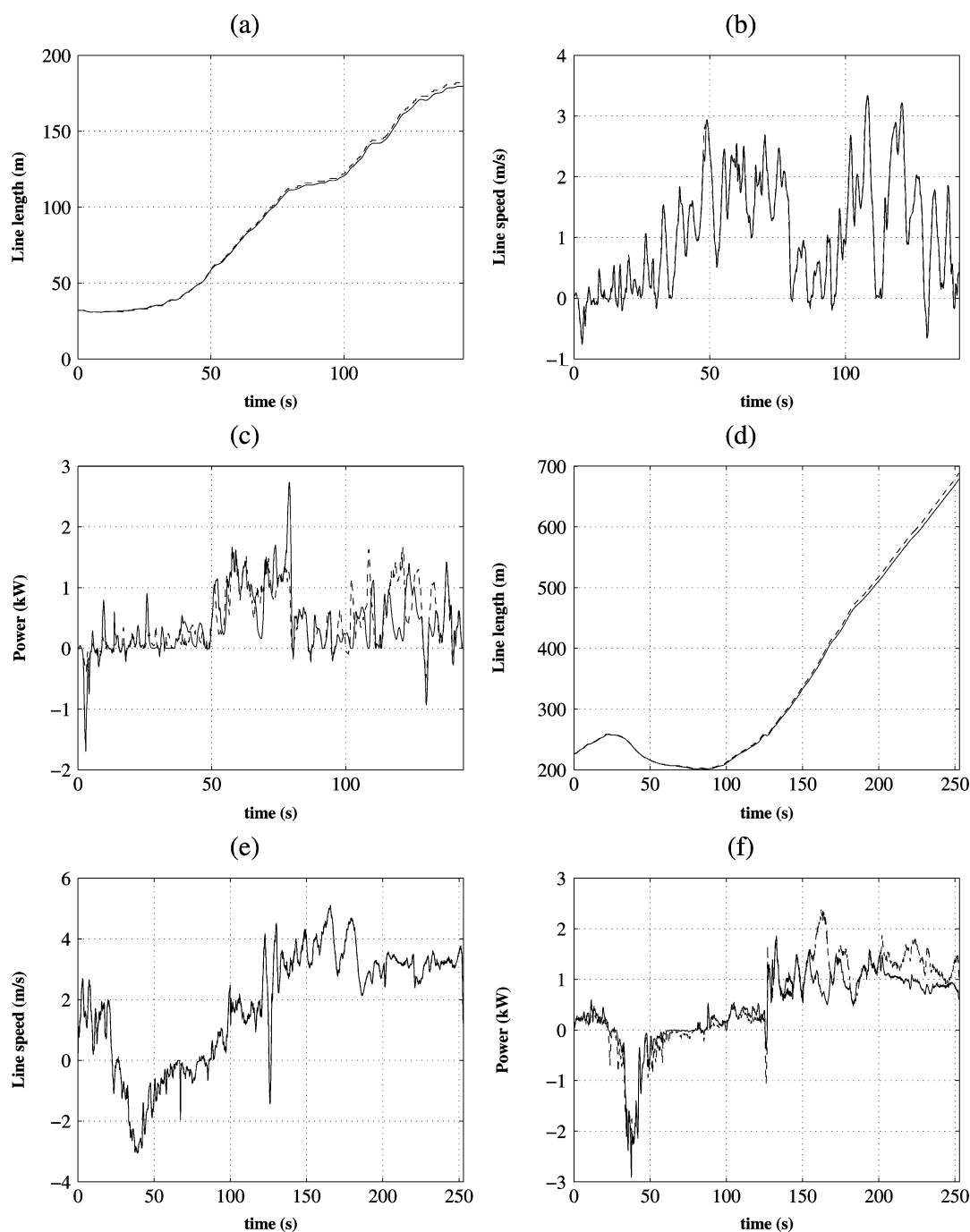


Fig. 16. Measured (dashed line) and simulated (solid line): (a) line length r ; (b) line speed \dot{r} ; and (c) generated power P regarding experimental tests carried out in Sardegna, Italy, September 2006. Measured (dashed) and simulated (solid line): (d) line length r ; (e) line speed \dot{r} ; and (f) generated power P regarding experimental tests carried out near Torino, Italy, January 2008.

\$/MWh (depending on the size of the wind farm) is obtained with KiteGen, against the actual 150 \$/MWh of wind energy and 50–90 \$/MWh of fossil energy. This means that a KiteGen generator would produce more energy than a wind tower in the same site, with much lower construction and installation costs, making the cost of wind energy competitive with that of fossil energy, with no more longer need of economical incentives. Indeed, the presented study is only preliminary and it does not take into account technological implementation problems. However, it is expected that the industrialization

of high-altitude wind energy may require from 3 to 5 years, since no further basic research or technological innovations are needed, but only the fusion of advanced competencies already available in different engineering fields, such as modeling and control, aerodynamics and flight mechanics, materials and mechatronics.

REFERENCES

- [1] C. L. Archer and M. Z. Jacobson, "Evaluation of global wind power," *J. Geophys. Res.*, vol. 110, 2005, D12110.

- [2] R. Thresher, M. Robinson, and P. Veers, "To capture the wind," *IEEE Power Energy Mag.*, vol. 5, no. 6, pp. 34–46, 2007.
- [3] M. Canale, L. Fagiano, M. Milanese, and M. Ippolito, "Control of tethered airfoils for a new class of wind energy generator," in *Proc. 45th Conf. Dec. Control*, 2006, pp. 4020–4026.
- [4] M. Canale, L. Fagiano, and M. Milanese, "Power kites for wind energy generation," *IEEE Control Syst. Mag.*, vol. 27, no. 6, pp. 25–38, Jun. 2007.
- [5] M. Canale, L. Fagiano, and M. Milanese, "Kitegen: A revolution in wind energy generation," *Energy*, vol. 34, no. 3, pp. 355–361, 2009.
- [6] A. Ilzhöfer, B. Houska, and M. Diehl, "Nonlinear mpc of kites under varying wind conditions for a new class of large-scale wind power generators," *Int. J. Robust Nonlinear Control*, vol. 17, pp. 1590–1599, 2007.
- [7] P. Williams, B. Lansdorp, and W. Ockels, "Optimal crosswind towing and power generation with tethered kites," *J. Guid., Control, Dyn.*, vol. 31, pp. 81–93, 2008.
- [8] M. Canale, L. Fagiano, and M. Milanese, "Fast nonlinear model predictive control using set membership approximation," in *Proc. 17th IFAC World Congr.*, Seoul, South Korea, 2008, pp. 12165–12170.
- [9] M. Canale, L. Fagiano, and M. Milanese, "Set membership approximation theory for fast implementation of model predictive control laws," *Automatica*, vol. 45, pp. 45–54, 2009.
- [10] B. Houska and M. Diehl, "Optimal control for power generating kites," in *Proc. 9th Eur. Control Conf.*, Kos, Greece, 2007, pp. 3560–3567.
- [11] M. Diehl, "Real-time optimization for large scale nonlinear processes," Ph.D. dissertation, Interdisciplinary Inst. for Scientific Comput. (IWR), Univ. Heidelberg, Heidelberg, Germany, 2001.
- [12] G. M. Maneia, "Aerodynamic study of airfoils and wings for power kites applications," Master's thesis, Politecnico di Torino, Torino, Italy, Oct. 2007.
- [13] D. Q. Mayne, J. B. Rawlings, C. V. Rao, and P. Scokaert, "Constrained model predictive control: Stability and optimality," *Automatica*, vol. 36, pp. 789–814, 2000.
- [14] M. Canale, L. Fagiano, and M. Milanese, "On the use of approximated predictive control laws for nonlinear systems," in *Proc. 47th IEEE Conf. Dec. Control*, Cancun, Mexico, 2008, pp. 4712–4717.
- [15] Control Comput. Dept., Politecnico di Torino, Torino, Italy, "Complex systems modeling and control group website," 2009. [Online]. Available: <http://www.polito.it/modelingcontrol/>
- [16] National Oceanographic and Atmospheric Administration, Earth System Research Lab., Boulder, CO, "NOAA/ESRL radiosonde database access," 2009. [Online]. Available: <http://raob.fsl.noaa.gov/>



Massimo Canale (M'06) received the Laurea degree in electronic engineering and the Ph.D. degree in systems engineering from the Politecnico di Torino, Torino, Italy, in 1992 and 1997, respectively.

From 1997 to 1998, he worked as a Software Engineer in the R&D Department, Comau Robotics, Italy. Since 1998, he has been an Assistant Professor with the Dipartimento di Automatica e Informatica, Politecnico di Torino. His research interests include robust control, model predictive control, set membership approximation, and application to automotive

and aerospace problems.

Dr. Canale is a member of the IEEE Technical Committee on Automotive Control.



Lorenzo Fagiano (M'07) received the Bachelor's degree in automotive engineering, the Master's degree in automotive engineering, and the Ph.D. degree in information and system engineering from Politecnico di Torino, Torino, Italy, in 2002, 2004, and 2009.

In 2005, he worked for Fiat Research Centre, Italy, in the active vehicle systems area. Currently, he holds a post-doctoral position at Politecnico di Torino. His main research interests include constrained robust and nonlinear control and set membership theory for

control purposes, applied to automotive control and the KiteGen project.



Mario Milanese (M'90–SM'04) graduated in electronic engineering at Politecnico di Torino, Torino, Italy, in 1967.

Since 1980, he has been a full Professor of system theory at Politecnico di Torino. From 1982 to 1987, he was head of the Dipartimento di Automatica e Informatica, Politecnico di Torino. His research interests include identification, prediction, and control of uncertain systems with applications to biomedical, automotive, aerospace, financial, environmental, and energy problems. He is the author of over 200 papers

in international journals and conference proceedings.